CHEMISTRY
A European Journal

A Journal of
ChemPubSoc Europe

Accepted Article

Title: [FeFe]-Hydrogenase H-Cluster Mimics with Unique Plan
SCH2)2ER2 Linkers (E = Ge and Sn)

Authors: Wolfgang Weigand, Hassan Abul-Futouh, Laith R.
Almazahreh, Takahiro Sakamoto, Nhu Y T. Stessma
L. Lichtenberger, Richard S. Glass, Mohammad El-k
Philippe Schollhammer, and Grzegorz Mloston

To be cited as: *Chem. Eur. J.* 10.1002/chem.201603843

Link to VoR: http://dx.doi.org/10.1002/chem.201603843


WILEY-VCH

FULL PAPER

WILEY-VCH

[FeFe]-Hydrogenase H-Cluster Mimics with Unique Planar ($\mu SCH_2)_2ER_2$ Linkers (E = Ge and Sn)

Hassan Abul-Futouh,[a] Laith R. Almazahreh,*[a] Takahiro Sakamoto,[b] Nhu Y T. Stessman,[b] Dennis L. Lichtenberger,*[b] Richard S. Glass,*[b] Mohammad El-khateeb,[c] Philippe Schollhammer,*[d] Grzegorz Mloston,[e] and Wolfgang Weigand*[a]

Abstract: Analogues of the [2Fe-2S] subcluster of hydrogenase enzymes in which the central group of the three-atom chain linker between the sulfur atoms is replaced by GeR_2 and SnR_2 groups are studied. The six-membered FeSCECS rings in these complexes (E = Ge or Sn) adopt an unusual conformation with nearly coplanar SCECS atoms perpendicular to the Fe–Fe core. Computational modelling traces this result to steric interaction of the Me groups with the axial carbonyls of the $Fe_2(CO)_6$ cluster and low torsional strain for $GeMe_2$ and $SnMe_2$ moieties due to the long C–Ge and C–Sn bond lengths. Gas phase photoelectron spectroscopy of these complexes shows a shift of ionizations with substantial sulfur orbital character to lower energies and, as supported by the computations, an increase in sulfur character in the predominantly metal-metal bonding HOMO. Cyclic voltammetry reveals that the complexes follow an ECE-type reduction mechanism in the absence of acid, and catalysis of proton reduction in the presence of acid. Two cyclic cluster dimers featuring the sulfur atoms of two $Fe_2S_2(CO)_6$ cores bridged by $CH_2SnR_2CH_2$, R = Me, Ph, linkers were also obtained and characterized.

Introduction

The active H-cluster site of [FeFe]-hydrogenases (Figure 1) contains a [2Fe-2S] subcluster with a semi-bridging carbonyl ligand between the iron centers.[1] This semi-bridging orientation of the carbonyl ligand is thought to be important because it opens an axial site on the iron atom that is distal to the [4Fe-4S] cubane subcluster for protonation of the iron center. DFT studies have proposed that protonation of the azadithiolate linker μSCH_2NHCH_2S at the NH[1,2] group or protonation of the μ-S atoms[3] provides low energy kinetic pathways for protonation of the axial site and dihydrogen formation, which occurs with the enzyme at a midpoint potential of -0.42 V (vs NHE)[4] at pH = 8.0, which is close to the thermodynamic potential. Proton relay to the vacant axial iron site via agostic or hydrido-proton interaction from the azadithiolate linker to the iron is thought to be responsible for the high efficiency of catalytic hydrogen release by the H cluster (ca. 10^4 turnover/s).[1,2,5]

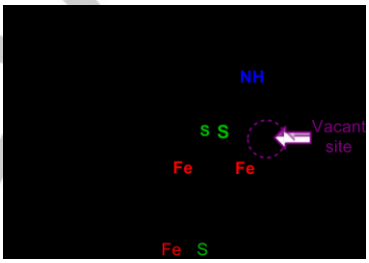

Figure 1. The active H-cluster site of a [FeFe]-hydrogenase.[1]

Models for the active site [2Fe-2S] subcluster have been extensively studied.[6] Although mixed valence analogues with a semibridging carbonyl and rotated structure have been reported,[7] the Fe(I)Fe(I) models typically do not exhibit these essential features. However, three complexes with these features have been reported.[8] To adopt these features up to three requirements were denoted: (i) bulkiness of the dithiolato bridge, (ii) desymmetrization of the di-iron system and (iii) agostic interaction in two cases. Bulkiness in the dithiolato bridge was previously proposed to favor these geometric changes on the basis of computations[9] and, owing to steric interactions between a methyl group and an apical CO in $Fe_2(CO)_6\{(\mu\text{-}SCH_2)_2CMe_2\}$, the $Fe(CO)_3$ moiety is twisted.[10] It should be noted that the $CH_2CMe_2CH_2$ bridge adopts a bent geometry such that the $FeS_2(CH_2)_2CMe_2$ ring may be described as a chair conformation with respect to one Fe and a boat conformation with respect to the other Fe. Furthermore, this chair/boat conformation undergoes ring inversion in analogy with cyclohexane. Even in [2Fe-2S] models with all terminal CO ligands acting as electrocatalysts for H_2 production from weak acids, the core reorganization may play a critical role. For example, potential inversion, in which the first $1e^-$ reduction potential is more negative than second $1e^-$ reduction potential, occurs if there is an intervening reorganization.[11]

[a] Institut für Anorganische und Analytische Chemie, Friedrich-SchillerUniversität Jena, Humboldt Str. 8, 07743 Jena, GERMANY Email: wolfgang.weigand@uni-jena.de
[b] Department of Chemistry & Biochemistry, The University of Arizona, Tucson, AZ, 85721, U.S.A. Email: rglass@email.arizona.edu dlichten@email.arizona.edu
[c] Chemistry Department, Jordan University of Science and Technology, Irbid 22110, Jordan. Email: kateeb@just.edu.jo
[d] UMR CNRS 6521, Université de Bretagne Occidentale, 6 avenue Le Gorgeu, C.S. 93837, 29238 Brest-Cedex, France. Email: philippe.schollhammer@univ-brest.fr
[e] Section of Heteroorganic Compounds, University of Lodz, Narutowicza 68, 90-136, Lodz, Poland. Email: gmloston@uni.lodz.pl

Supporting information for this article is given via a link at the end of the document.

The synthetic models related to the structure of the Hcluster may be divided into two categories: (i) Bioinspired models with azadithiolato linkers[12] and (ii) artificial models with abiological linkers μ-$(XCH_2)_2Y$ in which the central atom/group Y is CR_2,[3d,12o,13] O,[13d,14] S,[15] Se,[16] SiR_2[3e,17] or Ph-P=O[18] and X could be S[12-18], Se[19], Te[19c,19d] or PR[20]. The use of these abiological linkers may provide valuable information and answers to basic questions concerning the role of the dithiolato bridge as well as the effect of the unusual Y on the structural and functional properties of such artificial H cluster mimics. For example, Goy et al. recently reported a model with an especially bulky Si-containing moiety, namely $Fe_2(CO)_5(PPh_3)\{(\mu SCH_2)_2Si(1\text{-silafluorene})\}$.[3e] In this case, protonation of the sulfur atoms by triflic acid is favored by an interplay of the presence of the Si atom, the steric bulkiness of the Si-containing moiety and the presence of one σ-donor PPh_3 ligand at the diiron core. Previous suggestions of the relevance and observation of protonation at sulfur have been made.[3] In addition, we have previously shown that the electron richness of thioether moieties, as judged by ionization energies determined by photoelectron studies on $Fe_2(CO)_6\{(\mu\text{-}SCH_2)_2SnR_2\}$ complexes[21] and other compounds with SCSn groups,[22] is dramatically increased by a C-Sn bond owing to a geometrydependent σ(Sn-C)↔3p(μ-S) filled-filled interaction.

We report in the present paper the synthesis of models with μ-$(SCH_2)_2ER_2$ linkers, where the central atom E is Ge or Sn. Here the steric hindrance can be varied by judicious choice of R. We now study in a systematic manner the molecular structures and electronic structures of a series of complexes depicted in Scheme 1, where complexes **1** (R = H or Me)[10b,13c] and **2** (R = Me)[17] have been reported previously.

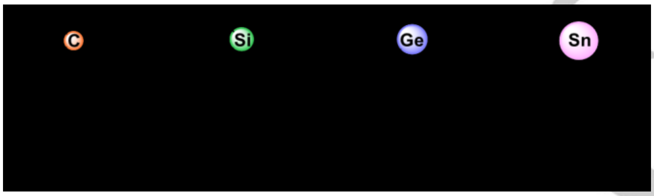

Scheme 1. A series of [FeFe]-hydrogenase mimics containing group IV elements with increasing size of bridgehead atoms in the dithiolate linker. The drawings do not depict the variations in the geometries of the linkages and the $Fe_2(CO)_6$ portions of the structures that are revealed in this study.

This series provides insight into the effect of Ge and Sn on the molecular structure of the Fe(I)Fe(I) complexes and their reorganization energies on forming formal Fe(I)Fe(II) ions, as well as the effect of the C–Ge and C–Sn bonds on the electronrichness of the adjacent S atoms. Within the series in Scheme 1, only the models **3** and **4** reveal a unique planarity when R = Me, also in comparison to all of the previously reported models that show the usual chair/boat conformation of the two fused FeS_2C_2E rings. We herein illuminate the origin of the planarity and its impact on the electron richness of the S atoms. Furthermore, we report the effect of germanylation and stannylation on the redox properties and describe the electrocatalytic behavior of these complexes toward reduction of protons from moderate and strong acids.

Results and Discussion

Synthesis and Characterization of $R_2Sn(CH_2I)_2$

The compound $Ph_2Sn(CH_2I)_2$ was synthesized following a similar procedure applied for $Me_2Sn(CH_2I)_2$.[23] The reaction of Ph_2SnCl_2 with two equiv. of *in situ* generated $IZnCH_2I$ afforded $Ph_2Sn(CH_2I)_2$ in ca. 48% yield after purification by column chromatography as a colorless liquid (Scheme 2).

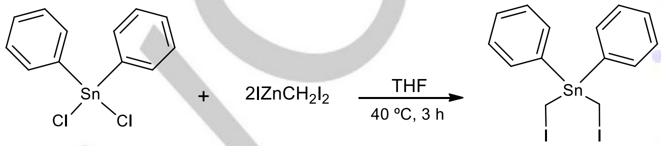

Scheme 2. Synthesis of $Ph_2Sn(CH_2I)_2$.

The compound $Ph_2Sn(CH_2I)_2$ was characterized by ^1H and $^{13}C\{^1H\}$ NMR spectroscopy and mass spectrometry. Its ^1H NMR spectrum ($CDCl_3$, 400.08 MHz) exhibits a singlet at 2.41 ppm with Sn satellites ($^2J\{^{117}Sn,^1H\}$ = 20.9 Hz and $^2J\{^{119}Sn,^1H\}$ = 41.8 Hz) for the CH_2 hydrogen atoms. The hydrogen atoms at the meta and para positions of the Ph groups show a multiplet in the region of 7.38-7.43 ppm and the hydrogen atoms located at the ortho position resonate in the region of 7.55-7.60 ppm. The $^{13}C\{^1H\}$ NMR spectrum shows a singlet at -10.53 ppm due to the CH_2 carbon atoms. The Ph groups show multiplets at 126.0128.8 (meta and para C atoms), 136.85 ppm (ortho C atoms) and 139.31 ppm (ipso C atoms) in the $^{13}C\{^1H\}$ NMR spectrum. In addition, the DEI-MS spectrum shows peaks at *m/z* 479 $[PhSn(CH_2I)_2]^+$, 415 $[Ph_2SnCH_2I]^+$, 351 $[PhSn(CH_2I)(CH_2)]^+$ and 273 $[Ph_2Sn]^+$.

Synthesis and Characterization of the Iron Complexes

The reaction of *in situ* generated $(\mu\text{-}LiS)_2Fe_2(CO)_6$ with one equivalent of $R_2Sn(CH_2I)_2$ afforded $Fe_2(CO)_6\{(\mu\text{-}SCH_2)_2SnR_2\}$ (R = Me, **4a**, 25 % yield and Ph, **4b**, 18 %) as air-stable red solids as well as unexpected tetranuclear products $[Fe_2(CO)_6\{(\mu SCH_2)_2SnR_2\}]_2$ (R = Me, **5a**, 9 % yield, and R = Ph, **5b**, traces) as air-stable orange solids (Scheme 3). On the other hand, we were able to isolate only $Fe_2(CO)_6\{(\mu\text{-}SCH_2)_2GeMe_2\}$ (**3**) in 15 % yield from the reaction of $(\mu\text{-}LiS)_2Fe_2(CO)_6$ with one equivalent of $Me_2Ge(CH_2Cl)_2$, but not a tetranuclear product. Complexes **3**, **4a**, **4b**, and **5a** were characterized by means of ^1H, $^{13}C\{^1H\}$ NMR and IR spectroscopic techniques as well as mass spectrometry, elemental analysis and X-ray crystallography. Because of the very low yield of **5b**, we were only able to characterize it by Xray crystallography.

Scheme 3. Syntheses of complexes **3**-**5b**.

The dinuclear complex 3. The ESI-MS spectrum of **3** shows the parent ion peak at *m/z* 476 $[M]^+$ as well as the consecutive loss of the CO ligands at *m/z* 448 $[M - CO]^+$, 420 $[M - 2CO]^+$, 392 $[M - 3CO]^+$, 364 $[M - 4CO]^+$, 334 $[M - 5CO]^+$ and 308 $[M - 6CO]^+$. The IR spectrum (CH_2Cl_2 solution) of **3** displays four absorption bands at υ(CO) = 1990 (s), 1998 (s), 2032 (vs) and 2071 (s) cm^{-1} for terminal CO ligands. The $^{13}C\{^1H\}$ NMR spectrum of **3** exhibits singlets at 0.13, 6.5 and 207.95 ppm for the *C*H_3, *C*H_2 and *C*O carbon atoms, respectively. In the ^1H NMR spectrum, two singlets are observed at 0.26 and 1.66 ppm due to the C*H*$_3$ and C*H*$_2$ protons, respectively.

The dinuclear complexes 4a and 4b. The DEI-MS spectra of **4a** and **4b** show the parent ion peak at *m/z* 520 $[M]^+$ and 646 $[M]^+$, respectively, as well as the consecutive loss of the CO ligands. The IR spectrum (CH_2Cl_2 solution) of **4a** displays four vibration bands at υ(CO) = 1989 (s), 1997 (s), 2032 (vs) and 2070 (s) cm^{-1} whereas three υ(CO) bands are observed at 1989 (vs), 2033 (vs) and 2066 (s) cm^{-1} in case of **4b**. The υ(CO) wavenumbers (CH_2Cl_2 solution) slightly shift to smaller values ongoing from **1** (R = Me; 1990 (s), 2000 (s), 2032 (vs), 2073 (s) cm^{-1}), **2** (R = Me; 1990 (s),1998 (s), 2032 (vs), 2072 (s) cm^{-1}) and **3** to **4a**. The $^{13}C\{^1H\}$ NMR spectrum of **4a** shows singlets at -7.1, 1.6 and 207.0 ppm for the *C*H_3, *C*H_2 and *C*O carbon atoms; respectively, while that of **4b** exhibits a singlet at 1.7 ppm for the *C*H_2 groups as well as peaks due to the Ph substituents in the region of 128.7-130.6 ppm (meta and para C atoms) and 136.7138.7 ppm (ipso and ortho C atoms). The CO ligands of **4b** resonate at 208.6 and 209.1 ppm, which is in contrast to the $^{13}C\{^1H\}$ NMR spectrum of **4a** that shows only one signal due to the CO ligands. The ^1H NMR spectra of **4a** and **4b** exhibit a singlet at 1.79 ppm (**4a**) and 2.27 ppm (**4b**), respectively, for the C*H*$_2$ protons. Complex **4a** shows a singlet at 0.25 ppm due to the C*H*$_3$ protons in the ^1H NMR spectrum, while the spectrum of complex **4b** displays a multiplet in the region of 7.35-7.70 ppm attributed to the Ph protons.

each iron core of **3**, **4a** and **4b** can be best described as a distorted octahedron in which the central atom is Fe surrounded by three terminal CO ligands in facial fashion as well as two S atoms that bridge both iron atoms. The bicyclic [2Fe-2S] structure in these complexes reveals a butterfly conformation. The bridgehead E atoms of the linker μ-$(SCH_2)_2ER_2$ (ER_2 = $GeMe_2$, $SnMe_2$, $SnPh_2$) of the complexes is surrounded by atoms in distorted tetrahedral fashion.

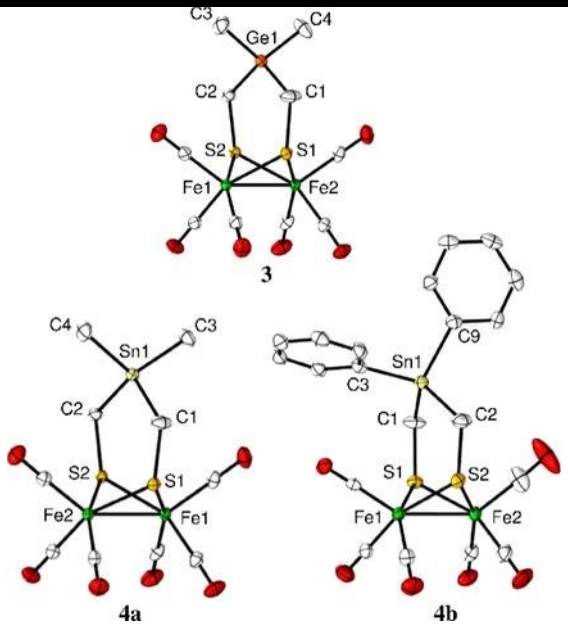

Figure 2. Molecular structures (50% probability) of **3**, **4a** and **4b**.

The average E-C-S bond angles (122.42(13)º (**3**), 121.96(15)º (**4a**) and 119.7(2)º (**4b**)) deviate significantly from the ideal tetrahedral angle as was observed in various $Fe_2(CO)_6\{(\mu\text{-}SCH_2)_2SiR_2\}$ models, 118.22(12)-122.05(13)º.[17]

The Fe-Fe bond lengths in **3** (2.5128(4) Å), **4a** (2.5249(5) Å) and **4b** (2.5158(7) Å) are slightly shorter than those of the H-cluster, 2.55-2.62 Å,[2,24] but comparable to those in the complexes with the μ-$(SCH_2)_2SiR_2$ linker (ca. 2.518 Å).[17] The average Fe-CO bond lengths are 1.800(2), 1.802(3), and 1.798(4) Å in **3**, **4a**,

and **4b**, respectively. The average Fe-S bond lengths (2.2535(6) Å (**3**), 2.2561(8) Å (**4a**) and 2.2582(10) Å (**4b**)) are comparable to those in $Fe_2(CO)_6\{(\mu\text{-}SCH_2)_2SiMe_2\}$ (2.2582(6) Å).[17]

Geometry of the dithiolato linker

All of the previously reported [FeFe]-hydrogenase models adopt a chair/boat conformation (Figure 3) of the two fused sixmembered FeSCECS rings in the solid state as well as in solution and many complexes such as **1**, R = H or Me, undergo FeSCECS ring inversion[10b] with the E atom exchanging places on either side of the molecule. The flap angle (α) formed from the intersection between the C_2E and S_2C_2 planes, as shown in Figure 3, lies within the range of 118° > α > 160° in various [FeFe]-hydrogenase models. Only one complex, namely $Fe_2(CO)_6\{(\mu\text{-}SCH_2)_2Si(1\text{-silafluorene})\}$[3e], has a large angle α = 171°. In the sofa conformation α = 180º and the -SCECS- moiety is planar. Table 1 lists the flap angle α for the homologous series with CMe_2, $SiMe_2$, $GeMe_2$ and $SnMe_2$ in the bridge as well as angles related to the $Fe(CO)_3$ distortion and twisting. Remarkably, the -SCECS- moiety is nearly planar for E = Ge and Sn. That is, the flap angles α deviate by only 4.8° (E = Ge) and 6.4° (E = Sn) from planarity. In addition, their solution NMR spectra show equivalent Me groups for E = Ge and Sn. This may result from a planar structure or rapid equilibration (ring inversion) of nonplanar isomers (as observed in the room temperature ^{1}H NMR spectrum of **1**, R = Me)[10b]. However, the Me groups in **4a** remain equivalent even at -90°C.

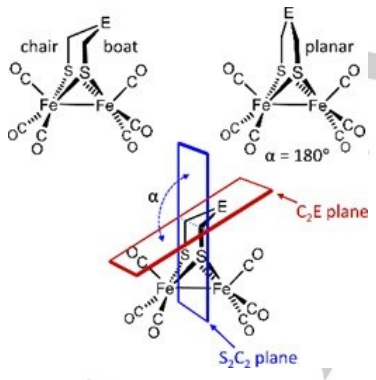

Figure 3. The chair/boat and planar conformations and the definition of the angle α.

To ascertain whether the variations in these structures are solid state effects or inherent to the molecules, the gas phase structures were computed and compared in Table 1 and S-1 for the lowest energy conformers. When R is Me, there is a general increase in the flap angle α for E going down the group with an angle of about 135° when E = C and approaching nearly 180° when E = Ge (only in the solid state structure), E = Sn (in both of the solid and gas phase structures). The flap angle in the molecular structure for the molecule with $ER_2 = GeMe_2$ seems anomalous, being slightly greater than the angle for $ER_2 = SnMe_2$, but examination of the crystal packing suggests that intermolecular interactions are influencing this angle in the solid state. This suggestion is supported by computation of the distortion energies. The gas phase structures (computational) reproduce the flap angles observed in the solid state structures within 2° for E = C, Si, and Sn, and place the flap angle for E = Ge intermediate to those for Si and Sn. The computations also account well for the solution carbonyl stretching frequencies (Figure S-1). These results indicate that the large flap angles for the heavier elements of group IV are an inherent property of the isolated molecules, but can be influenced by solid state packing forces especially for E = Ge and Sn.

The change in the R group also has a significant influence on the structure. When E = Sn, the flap angle α for R = Ph is about 20° less than that for R = Me. It is noted in the solid state structure of **4b** that one phenyl group is oriented approximately edge-on to an apical carbonyl while the other is face-on to the other apical carbonyl. The computations reproduce this orientation, but give a larger flap angle than observed in the solid state structure, and here again the crystal packing indicates intermolecular interactions between the phenyl rings are also at play. When E = C the comparison for R = H with R = Me is problematic because of disorder in the structure with CH_2 as the central bridge group. The gas phase structures obtained computationally give a much smaller flap angle of 126.6° for R = H than for R = Me, which is close to the ideal angle of 127° for a perfectly staggered conformation of a cyclohexane ring. Taken together the above observations indicate that steric factors play a major role in determining the flap angle α. As a computational test for E = Sn, the R groups were changed to H atoms, and the optimum -SCSnCS- structure bent substantially from planarity (Table 1).

The steric characteristics of the ER_2 groups distort the symmetry of the $Fe_2(CO)_6$ portion of the molecules. This is reflected in the bending of an apical carbonyl away from steric interaction with the ER_2 group and a rotation of an $Fe(CO)_3$ group away from the mirror plane of the molecule. The Fe-Fe-C(O) angles and (O)C-Fe-Fe-C(O) dihedral angles for the apical carbonyls of these molecules are listed in Table 1. The steric effect of the ER_2 group on the metal carbonyl is observed most clearly in the deflection of the apical carbonyl that is proximal to the ER_2 group. As pointed out previously by Darensbourg,[10] there is an appreciable increase in the distortion from $ER_2 = CH_2$ to CMe_2. Unfortunately, the disorder in the solid state structure for $ER_2 = CH_2$ prevents comparison of

Table 1. Influence of ER_2 groups (E = group IV element) toward planarity of the S_2C_2E linker and distortion of the $Fe_2(CO)_6$ symmetry in $Fe_2(CO)_6\{(\mu\text{-}SCH_2)_2ER_2\}$ complexes.

ER_2	CH_2	CMe_2	$SiMe_2$	$GeMe_2$	$SnMe_2$	$SnPh_2$	SnH_2
			Solid Phase Structures				
Flap angle α,[a] °	137.1[d]	135.7	150.0	175.2	173.6	152.5	–
Fe–Fe–C(O) [b], °	148.3/148.3[d] Δ = NA[d]	159.9/148.1 Δ = 11.8	152.8/144.7 Δ = 8.1	147.4/146.4 Δ = 1.0	146.2/145.1 Δ = 1.1	149.5/144.4 Δ = 5.1	–
C_a–Fe–Fe–C_a [c], °	0.0[d]	6.5	0.0	7.9	5.2	7.5	–
			Gas Phase Structures (Computational)				
Flap angle α, °	126.6	137.5	148.0	159.6	172.8	161.6	141.9
Fe–Fe–C_{CO} [a], °	151.5/146.0 Δ = 5.5	159.2/146.1 Δ = 13.1	154.1/144.0 Δ = 10.1	149.2/144.1 Δ = 5.1	144.8/142.8 Δ = 2.0	148.6/142.9 Δ = 5.7	151.0/144.3 Δ = 6.7
C_a–Fe–Fe–C_a [b], °	0.0	0.8	2.2	0.3	0.1	0.1	0.6

[a] See Figure 3 for illustration of the flap angle α. [b] Fe–Fe–C angle for the apical carbonyl proximal to the ER_2 group / Fe–Fe–C angle for the apical carbonyl distal to the ER_2 group (see Figure 4), Δ is the difference between these angles. [c] Dihedral twist angle of the apical carbonyl carbon atoms across the Fe–Fe bond. [d] Disorder in the crystal for the case of $ER_2 = CH_2$ averages the structure to C_{2v} symmetry, which masks any symmetry distortion.

the deflection of the carbonyls proximal and distal to the CH_2 group. However, the computations support the increasing deflection of the proximal carbonyl from the CH_2 to the CMe_2 complex. The dimethyl complexes show that the deflection of the apical carbonyl decreases from E = C to Si to Ge to Sn, both in the molecular structures and in the gas phase structures from the computations.

A deeper insight into the factors that determine this trend is obtained by imagining a split of the molecules into the dithiolato bridges and the $Fe_2(CO)_6$ fragments and computing the distortion energies of each fragment, as depicted in Figure 4. These distortion energies are thus in the absence of mutual steric and electronic effects between the fragments. The fragments are terminated by hydrogen atoms to satisfy the valence. The flap angle α of the linker is varied from 127°, which is the optimum angle of a fully staggered chair-like conformation, to 180°. Note that at α = 180° the E-C bonds of the EMe_2 groups are in a fully eclipsed conformation with the C-H bonds of the CH_2 groups. For CMe_2, the planar structure of the linker with the eclipsed bonds is disfavored by 7.7 kcal/mol, but this value falls by more than half for each substitution down the group ($SiMe_2$, 2.8; $GeMe_2$, 1.3 kcal/mol; $SnMe_2$, 0.5 kcal/mol). The dramatic decrease in this strain energy for the planar structures is attributed primarily to the longer E-C bonds that diminish the eclipsed non-bonded repulsions.

The EMe_2 groups are within van der Waals distance interactions with the axial carbonyls of the $Fe_2(CO)_6$ fragment even at the planar geometries. The optimized structures in which the linkers are constrained to be planar give distances from the hydrogen atoms of EMe_2 atom to the axial carbonyl O atom of 2.86 Å for CMe_2, 2.87 Å for $SiMe_2$, 2.88 Å for $GeMe_2$, and 2.94 Å for $SnMe_2$, whereas the van der Waals distance between these atoms implemented in the MM3 force field[25] is 3.44 Å and in the UFF force field is 3.19 Å.[26] This interaction forces a mutual distortion of each fragment.

The bottom of Figure 4 shows the energy cost of distorting the $Fe_2(CO)_6$ portion of the molecule as a function of the axial FeFe-C(O) angle through the maximum values obtained in the crystal structures and computations. When EMe_2 is CMe_2, there is a strong driving force toward the staggered linker conformation (α = 127°) that pushes a distortion of the $Fe_2(CO)_6$ portion of the molecule. This driving force toward the staggered conformation of the linker rapidly diminishes down the group of $SiMe_2$, $GeMe_2$, and $SnMe_2$. The potential energies when EMe_2 is

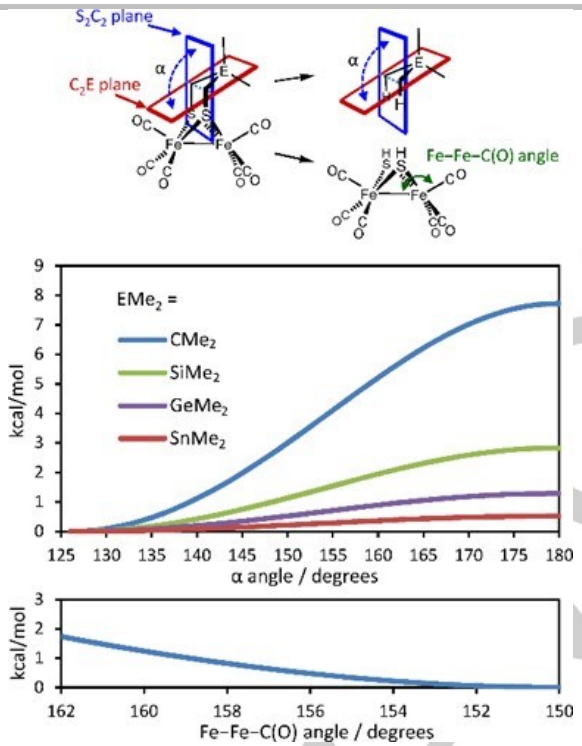

Figure 4. Top: illustration of the conceptual split of the molecule into the linker portion and the [2Fe-2S] portion for separate evaluation of the conformational energies, with definition of the distortion angle α from the fully staggered conformation (α = 127°) to the planar form (α = 180°) where the C-H bonds of the CH_2 groups are eclipsed with the E-C bonds of the EMe_2 group, and definition of the Fe-Fe-C(O) distortion angle. Middle: distortion energies of the linker as a function of the degree of planarity α. Bottom: distortion energy of the metal carbonyl as a function of the deflection of the proximal carbonyl away from the linker methyl group.

$GeMe_2$ and $SnMe_2$ are very flat in the region of α = 180°, making the structures obtained from crystal structures susceptible to packing forces as mentioned earlier.

Table 2 shows the calculated activation energies for the flap of the EMe_2 group from one side of the molecule to the other, in which the geometry where α = 180° is the transition state. For comparison, the case of CMe_2 has a smaller energy than the case of CH_2 in agreement with previous work.[10] The E = Si, Ge, and Sn cases have very small energies for the reasons given above, consistent with the low-temperature NMR spectrum. Geometries also were optimized using continuum solvation models for the NMR solvents THF, dichloromethane, and acetone, and these computations gave little difference in the relative conformational energies compared to the gas-phase computations.

ER_2	CH_2	CMe_2	$SiMe_2$	$GeMe_2$	$SnMe_2$
Flap	9.9	5.6	1.0	0.2	0.1
Rotate proximal	7.1	4.1	4.8	5.7	6.0
Rotate distal	10.4	10.8	10.1	5.6	5.9

The twist of the $Fe(CO)_3$ group gives a less clear indication of the steric interaction with the linker than the deflection of the axial carbonyl. The gas phase computations yield very little twist, and both the crystal structures and the computations do not show regular trends with increasing size of the ER_2 group. Nonetheless, the larger ER_2 groups may make the $Fe(CO)_3$ group more prone to rotation,

and the rotations found in the crystal structures may be sensitive to intermolecular interactions. Table 2 includes the calculated activation energies for rotation of the $Fe(CO)_3$ groups. For the familiar case of **1**, where ER_2 is CH_2, the computations

indicate the energy barrier for equilibration of the CO groups between axial and basal positions is about 10 kcal/mol, and this value compares well with the experimental activation energy of 10.4 kcal/mol determined from variable temperature NMR.[13c,27] Comparison of the energy for rotation of the $Fe(CO)_3$ group proximal to the ER_2 group of the linker with the rotation of the $Fe(CO)_3$ group distal to the ER_2 group gives an indication of the effect of the steric interaction of the ER_2 group. The smallest rotation energy for the proximal $Fe(CO)_3$ group and greatest difference from the rotation energy for the distal $Fe(CO)_3$ group is found for $ER_2 = CMe_2$. The Ge and Sn examples have essentially no difference between the proximal and distal $Fe(CO)_3$ rotation energies as expected from the near-planar geometries of these linkers.

The near planar geometries of the -SCECS- bridges in **3** and **4a** are remarkable in comparison to the conformations of cyclohexane. The six-membered FeSCECS moiety is comparable to the cyclohexane conformation with 5-coplanar atoms **A**. Although initially calculated by molecular mechanics[28] to be higher in energy than the half-chair conformation **B**, subsequent calculations suggest that they are comparable in energy[29] and provide the transition state for conversion of the chair to twist conformation[30] of cyclohexane with a 10.8 kcal/mol

barrier.[31] This is comparable to the 9.9 kcal/mol barrier for the similar process to **A** of the [2Fe-2S] complex with $ER_2 = CH_2$ shown in Table 2. Nevertheless, it is this conformation that is adopted in **4a** and almost as well in **3**. Previous studies on conformational analysis of cyclohexanes with higher Group IV elements in the ring are limited, but there have been studies on silacyclohexanes[32] as well as a silathia analogue[33], germacyclohexanes[34] and stannacyclohexanes[35]. The main conclusion of these studies is that there is a modest flattening of the chair conformation made possible by the greater C-Si than C-C bond length and consequent decease in Si-C repulsive torsional interactions as well as decreased ring inversion barriers. This flattening is taken to remarkable extremes in **4a** and **3**. It is interesting to note that Me···apical CO repulsion in **1** (R = Me) is predominantly relieved by $Fe(CO)_3$ geometry changes, but with **4a** and **3** it induces geometry changes in the -SCECS- flap. As mentioned previously in support of the Me···apical CO interaction as the driver in this distortion, calculations on **4** (R = H) are shown in Table 1 and reveal an α value of only 141.9°. Also note that comparison of the flap angles of **1** (R = H) and **1** (R = Me) reflect this interaction as well, although the molecular structures cannot be compared because of disorder in **1** (R = H).

Photoelectron Spectroscopy

Gas-phase ultraviolet photoelectron spectroscopy (UPS) offers a direct experimental probe of the valence electron energies in the absence of intermolecular interactions, and as such can provide information on the electronic structure variations through this series as the central bridgehead atom changes from C to Si to Ge to Sn. The technique is relevant to the study of hydrogenase mimics because the ionization of these molecules give direct access to the formal [Fe(I)Fe(II)] oxidation state in the proposed catalytic cycle of the enzyme.[2] In addition, the well-defined energy quantities provide experimental validation for the computational methods utilized in this study. The He I spectra of **1**-**3** (R = Me) in the energy region from 7 to 12 eV were collected and compared with the spectrum of **4a** from a previous study[21] in Figure 5.

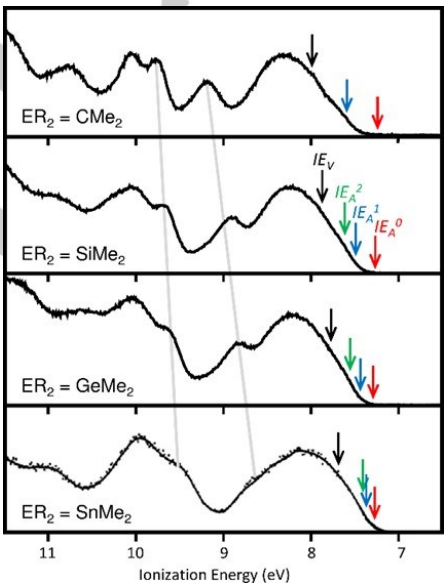

Figure 5. He I photoelectron spectra of **1**-**4a**. The black arrows point to the calculated vertical ionizations energies (IE_V). The red arrows correspond to the global minimum cation structures (IE_A^0), and blue and green arrows correspond to local minima (IE_A^1 and IE_A^2) of less stable cation structures (see text and Figure 7).

The He I UPS spectra and ionization band assignments of similar compounds have been reported previously.[19c,36] The broad first ionization band ranging from 7.5 to 8.7 eV represents the Fe-Fe σ bond and six occupied "t_{2g}-like" 3d orbitals that are oriented for backbonding to the carbonyl ligands on the two distorted-octahedral Fe centers, mixed with some S lone pair p orbitals. Ionization in the region from roughly 8.7 to 9.2 eV is primarily sulfur p in character mixed with significant Fe character, and another primarily sulfur p ionization is around 9.5 eV. The grey lines in Figure 5 trace the shift of these ionizations due to the neighboring effects from E = C to E = Sn.[21] Additional ionizations ranging from roughly 9.2 to 12.0 eV, consist of C, Si, Ge and Sn character interacting with S character and Fe d orbitals.

The leading edges of the first ionization bands correspond to ionizations from the HOMO, starting at about 7.5 eV for all molecules. The HOMOs of **1** (R = CMe_2) and **4a** (ER_2 = $SnMe_2$) are compared in Figure 6 (Figure S-2 for the HOMOs of **2**, R = Me, and **3**). In all cases the HOMO is primarily the Fe-Fe bond. In **1** the tilt of the CMe_2 group displaces the orbital more toward the distal Fe atom, whereas in **4a** the nearly planar linker between the S atoms (large α angle) creates a more symmetric orbital. Also note the increase in S character in the HOMO of **4a** with some antibonding interaction with the linker atoms, both of which can facilitate protonation of the [2Fe-2S] cluster. The S character in the HOMO increases in the series E = C, Si, Ge, Sn (Figure S-2) due to the increasing instability of the E orbitals and E–C sigma bonds that impart both an inductive and overlap destabilization of the S lone pair that then mixes with the metal-metal bond density in an antibonding fashion in the HOMO.

The calculated ionization energies corresponding to removal of an electron from the HOMO of these molecules are indicated by a series of arrows on the photoelectron spectra shown in Figure 5. The vertical ionization energies (IE_V), calculated by the ΔSCF difference in energy from the neutral molecule to the cation, without change in geometry, are found to decrease from 7.98 eV for **1** to 7.86 eV for **2** to 7.77 eV for **3** and to 7.68 eV for **4a** (Table 3). The adiabatic ionization energies (IE_A^0) of these compounds are calculated by the ΔSCF method with full geometry optimization of the cations as shown in Figure 7 for **4a**.

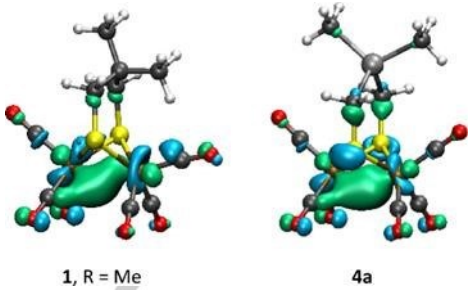

Figure 6. The HOMOs of **1**, R = Me, and **4a** (isosurface value ±0.05).

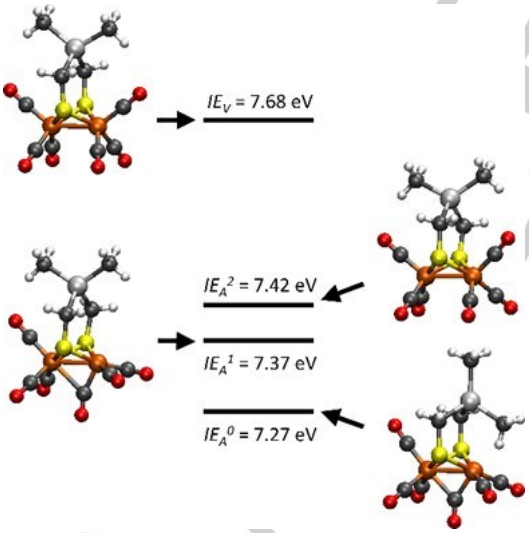

Table 3. Calculated first ionization energies and reorganization energies of $Fe_2(CO)_6\{(\mu\text{-}SCH_2)_2EMe_2\}$ complexes (all energies in eV).

[a]

ER_2	CMe_2	$SiMe_2$	$GeMe_2$	$SnMe_2$
IE_V	7.98	7.86	7.77	7.68
IE_{A0}	7.23	7.26	7.28	7.27
IE_{A1}	7.58	7.48	7.43	7.37
IE_{A2}	*N/A*[b]	7.61	7.52	7.42
λ[a]	0.75	0.60	0.49	0.41

Reorganization energy with ionization, $IE_V - IE_A^0$. [b] Local minimum for CMe_2 not available. Geometry relaxes automatically to the global minimum.

Figure 7. The cation structures and relative energies of **4a**, $Fe_2(CO)_6\{(\mu\text{-}SCH_2)_2SnMe_2\}$.

For all four complexes the global minimum IE_A^0 conformation of the cation has a rotated $Fe(CO)_3$ group with a bridging carbonyl and the dimethyl unit bends toward the vacant site. The alternative conformation (corresponding to IE_A^1) with the dimethyl unit in close proximity to the non-rotated apical terminal CO (Figure 7 for **4a** and Figure S-3 for molecules **1**-**3**) is a local minimum at higher energy. The difference in ionization energy from IE_A^1 to IE_A^0 for these two conformers is a combination of the stabilization gained from release

of the steric interaction of the linker with the apical carbonyl and the stabilization gained from the contribution of the agostic C-H bond to the Fe atom. The energy difference decreases down the series from E = C (0.35 eV) to Si (0.22 eV) to Ge (0.15 eV) to Sn (0.10 eV).

Another local minimum, IE_A^2, with an all terminal CO conformation was found for molecules **2**, **3**, and **4a**. However, all attempts to find a local minimum for the cation of molecule **1** (R = Me) with all terminal carbonyl ligands resulted in collapse to the global minimum conformation with the bridging carbonyl. This is a consequence of the stronger driving force to the rotated $Fe(CO)_3$ structure when ER_2 is CMe_2. The energy difference between the cation at the neutral molecule geometry (IE_V) and the optimized structure of the cation (IE_A^0) is the reorganization energy λ. Substantial reduction of reorganization energy was found, 0.75 eV for **1** (R = Me), 0.60 eV for **2**, 0.49 eV for **3** and 0.41 eV for **4a**, from C to Sn consistent with the indications of decreasing strain down the series.

The Tetranuclear Models

The X-ray diffraction analyses confirmed the tetranuclear structures of **5a** and **5b** as macrocycles in which each $Fe_2S_2(CO)_6$ unit has nonequivalent axial (*a*) and equatorial (*e*) $-CH_2-$ units (Figure 8). That is, the stereochemistry of the linkers connected to the sulfur atoms in **5a** is *e,a,e',a'* (the unprimed labels correspond to one [2Fe-2S] cluster and the primed labels to the other [2Fe-2S] cluster). While the average Fe–Fe, Fe–CO and Fe–S bond lengths in **5a** (2.5224(6), 1.797(3) and 2.2638(8) Å, respectively) and **5b** (2.5165(5), 1.803(3) and 2.2616(7) Å, respectively) are comparable to those in **4a** and **4b**, the Sn–C–S bond angles in **5a** (107.32(14)º-114.08(14)º) and **5b** (111.19(13)-112.33(13)º) are closer to the ideal tetrahedral angle. Examples of tetranuclear complexes in which two butterfly [2Fe-2S] clusters are part of a macrocycle are rare in the literature and are reported only when the dithiolato linker contains more than three atoms between the two sulfur atoms ($-S-CH_2-(X)_n-CH_2-S-$, n > 1).[37] In our case, the formation of these macrocycles (**5a** and **5b**) is allowed by the longer dithiolato linker chain $-S-CH_2-Sn-CH_2-S-$ due to the large size of the Sn atom and hence the relatively long Sn–CH_2 bond (average: 2.155(3) for **5a** and 2.156(3) for **5b** Å). Of particular relevance is the tetranuclear macrocycle **C**[37a] in which two $Fe_2S_2(CO)_6$ moieties are connected by $CH_2(CH_2OCH_2)_2CH_2$ units forming a 24membered ring with *e,a,e',a'*-stereochemistry similar to **5a**.

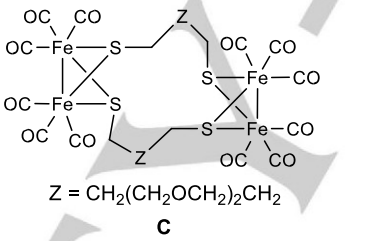

C

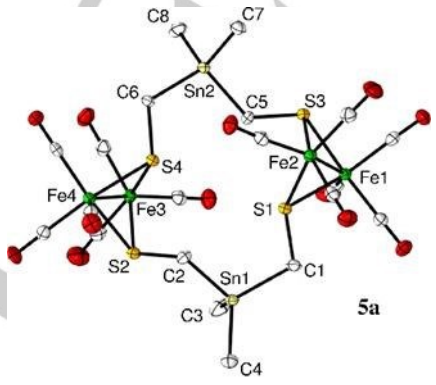

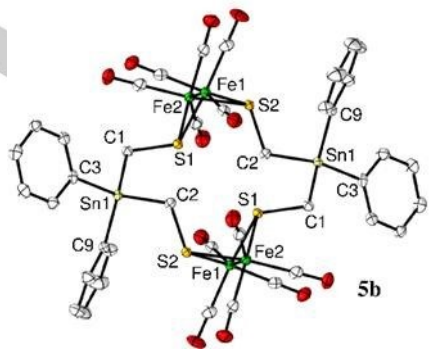

Figure 8. Molecular structures (50% probability) of complexes **5a** (to the top) and **5b** (to the bottom).

The structures of the $Fe_2S_2(CO)_6$ units of **5a** and **C** are comparable. However, there is a 14-membered ring in **5a** which results in the $Fe_2S_2(CO)_6$ units being much closer to each other than those in **C**. The intramolecular distances between Fe and S atoms in one unit and those in the other unit for **5a** are listed in Table S-3. As seen in Table S1, the shortest Fe···S distances are 4.841 and 4.874 Å. All of the Fe···S distances involving the Fe of one $Fe_2S_2(CO)_6$ and a S of the other cluster in **C** are greater than 7.39 Å. The molecular structure of **5a** shows that for each $Fe_2S_2(CO)_6$ unit there is an *a* and *e* CH_2 substituent. Nevertheless, its ^1H NMR spectrum shows a singlet for the CH_2 groups despite their nonequivalence. This observation is surprising because compound **D**[21], in which one CH_2SnMe_3 substituent is *a* and the other is *e*, shows two singlets for the nonequivalent CH_2 groups at room temperature.[38]

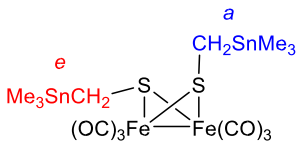

D

It is possible that the *a* and *e* positions in **5a** interconvert at room temperature. To test this possibility, we have performed VT ^1H NMR spectroscopic measurements and computational studies and found that the observation of one resonance signal arises from coincidental overlap of the temperature-dependent signals rather than interconversion of *a* and *e* substituents (for more details see the Supporting information, including Figure S-4).

Electrochemical Properties

Table 4 summarizes the electrochemical reduction and oxidation potentials from the cyclic voltammetric measurements of the complexes $Fe_2(CO)_6\{(\mu\text{-}SCH_2)_2EMe_2\}$ (**1**-**4a**). Complex **1**, R = Me shows the occurrence of only one quasi-reversible reduction, whereas complexes **2**-**4a** exhibit one partially reversible and one irreversible (irr.) reduction events at low scan rates. Increasing the scan rate *v* (see Figures 9 and S-5 to S-7) results in disappearance of the irreversible reduction event (the more cathodic peak in the cyclic voltammograms of **2**-**4a**) and an increase of the anodic-to-cathodic peak current ratio (I_{pa}/I_{pc}) of their first reduction wave. These observations can be readily explained in terms of irreversible follow-up reactions occurring after the first reduction process, forming side products.

Table 4. Summary of the redox features of complexes $Fe_2(CO)_6\{(\mu\text{-}SCH_2)_2EMe_2\}$ (**1**-**4a**) in 0.1 M CH_2Cl_2-[n-Bu_4N][PF_6] solution measured at v = 0.2 $V{\cdot}s^{-1}$ using glassy carbon disk (A = 0.072 cm^2). Potentials E are given in volts (V) and referenced to the ferrocenium/ferrocene couple (Fc^+/Fc).

Complex	E_{red1} [a]	$E_{1/2}$ [b]	E_{red2} [a]	$E_{ox,rot}$ [c]	E_{ox1} [d]
1	-1.75 (E_{pc}), -1.61 (E_{pa})	-1.68	–	+0.19	+0.81
2	-1.71 (E_{pc}), -1.61 (E_{pa})	-1.66	-1.84 (E_{pc}) irr.	+0.21	+0.77
3	-1.72 (E_{pc}), -1.62 (E_{pa})	-1.67	-1.85 (E_{pc}) irr.	+0.15	+0.74
4a	-1.68 (E_{pc}), -1.57 (E_{pa})	-1.62	-2.20 (E_{pc}) irr.	+0.13	+0.70

[a] E_{red1} and E_{red2} are the potentials for the first and the second reductions, where E_{pc} and E_{pa} are the cathodic and anodic scan peak potentials. [b] $E_{1/2}$

is the half-wave potential for the first reduction event. Because the I_{pa}/I_{pc} value (anodic to cathodic peak currents ratio) at 0.2 V·s^{-1} of the complexes **24a** is less than 1, the $E_{1/2}$ can be considered as approximated values. [c] $E_{ox,rot}$ is the potential of a weak oxidation peak attributed to initial oxidation to the rotated structure as discussed previously for related compounds.[19a] [d] E_{ox1} is the potential of the primary oxidation peak. A second oxidation peak (E_{ox2}) is observed for complexes **1**, **2** and **4a** as a shoulder at the first oxidation peak, where E_{ox2} is more positive than E_{ox1}.

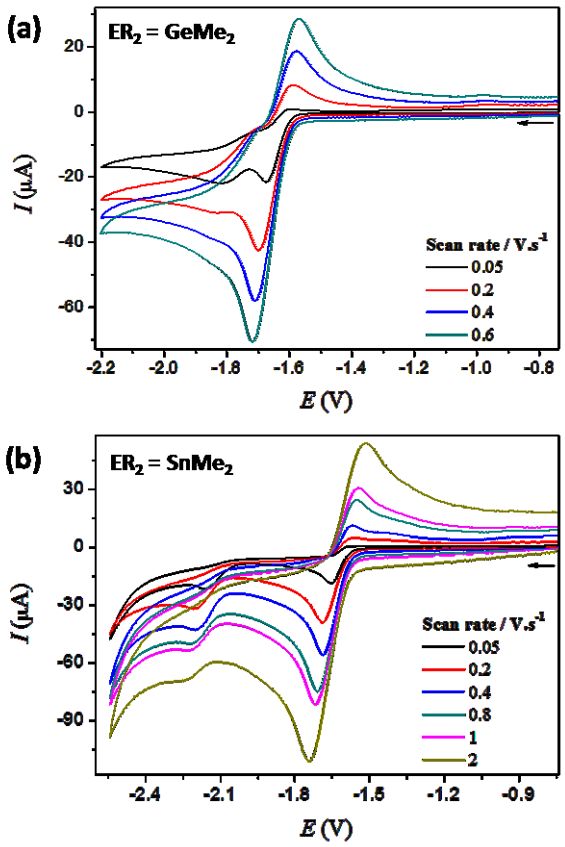

Figure 9. Cyclic voltammetry of (a) 0.84 mM $Fe_2(CO)_6\{(\mu\text{-}SCH_2)_2GeMe_2\}$ (**3**) and (b) 0.84 mM $Fe_2(CO)_6\{(\mu\text{-}SCH_2)_2SnMe_2\}$ (**4a**) in 0.1 M CH_2Cl_2-[n-Bu_4N][PF_6] solution under Ar at various scan rates. Glassy carbon electrode (A = 0.072 cm^2). E is in V against the Fc^+/Fc couple. The arrows indicate the scan direction.

The primary oxidation peak of these complexes (E_{ox1}) shows an overall cathodic shift of 110 mV on going from complex **1** to **2** to **3** to **4a**. This cathodic shift is a result of an increased electron density at the di-iron core and destabilization of the HOMO by the S lone pairs as discussed above, which eases the oxidation process. The potentials E_{ox1} correlate linearly with the computed vertical ionization energies from Table 3 with an excellent coefficient of determination R^2 = 0.995 (Figure S-11). Correlation of E_{ox1} with IE_v is consistent with a previous study of related compounds in which this oxidation event was attributed to initial oxidation to a species with all-terminal carbonyls similar to the structure of the neutral molecule.[19a] Also similar to the previous study, a very weak oxidation event is observed in the vicinity of 0.1 to -0.2 V that is consistent with oxidation to the cation with a rotated $Fe(CO)_3$ group and a bridging carbonyl ligand (Figure 7). The trend in this potential down the series is less dramatic and clearly due to the decreasing reorganization energies of the cations.

On going from **1** to **4a** the reduction potentials are less cathodic. That is, stannylated model **4a** is the easiest to reduce in comparison with the models **1**, **2** and **3**. This is due to reorganization and stabilization of the reduced species as previously shown in the case of electrochemical reduction of [FeFe]-hydrogenase models with [2Fe-2X] cores, where X = S, Se and Te.[6i,19] The reduction of the [2Fe-2X] core in this series of models becomes easier on going from X = S to Se to Te. Thus, these results show how the stannylation can tune the redox features of the [2Fe2S] core of the model complexes.

One important aspect of mechanistic investigation of proton reduction cycle catalyzed by a model complex is the determination of the number of electrons involved in the reduction of the model in the absence of a proton source. Studying the current function (I_{pc} / c·$v^{1/2}$, c = complex concentration) of the reduction process at slow and fast scan rates is a useful method to provide mechanistic information.[39] Figure 10 shows that the I_{pc} / c·$v^{1/2}$ value of the reduction of complexes **1**-**4a** starts to significantly increase as the scan rate decreases beyond 5 V·s^{-1}. This scan rate dependence of the current function suggests that the reduction of complexes **1**-**4a** follows an ECE-type mechanism at slow scan rates; E = electron transfer and C = chemical process.[6i,39,40] Based on theoretical and experimental studies on various [FeFe]-hydrogenase models including **1** and **2** as well, the intervening chemical process of the ECE reduction mechanism of **3** and **4a** might also involve similar core reorganization such that one Fe-S bond is broken and one $Fe(CO)_3$ unit rotates and locates one of its CO ligands in a semi-bridging position, leaving an open site at the iron atom.[6i,11,12b,17] We have recently illustrated how the steric clash between the CMe_2 group and the proximal CO in **1** lowers the barrier of $Fe(CO)_3$ rotation during the reduction process and hence leads to ECE reduction mechanism at slow scan rates. That the intervening core reorganization is a facile process during reduction of complexes **2**-**4a** can also be explained in terms of the steric bulkiness of their central EMe_2 groups of

the dithiolato linkers; notwithstanding the planarity of **3** and **4a** (see Table 2 for the barriers of $Fe(CO)_3$ rotation of the complexes in the ground Fe(I)Fe(I) states).[6i]

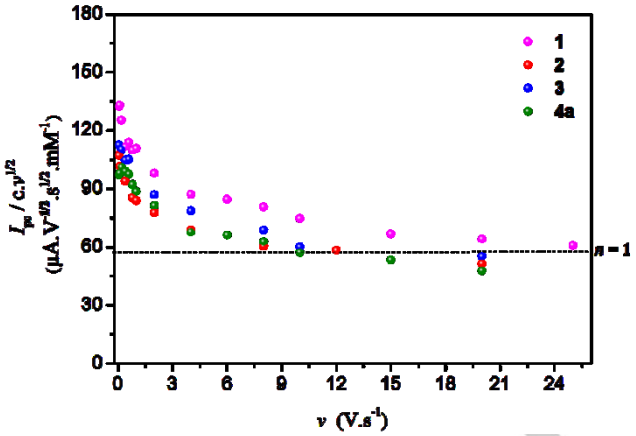

Figure 10. The scan rate dependence of the current function of the primary reduction peaks of complexes **1**-**4a** in 0.1 M CH_2Cl_2-[n-Bu_4N][PF_6] solution under Ar atmosphere. Glassy carbon electrode (A = 0.072 cm^2). The dashed line represents the current function expected for a one-electron process assuming $D \approx 9 \times 10^{-6}$ cm^2·s^{-1}, a value calculated for various [FeFe]-hydrogenase models[6i,18a].

Electrocatalysis

Furthermore, we have tested the electrochemical behavior of the models **3** and **4a** in the presence of the acids CF_3CO_2H (pK_a^{MeCN} = 12.7)[41] and CF_3SO_3H (pK_a^{MeCN} = 0.7)[41]. The presence of CF_3CO_2H in the solution of **3** (or **4a**) shifts their primary cathodic peak by ~110 mV to less negative potentials, which is a typical observation when protonation of a reduced species takes place.[3e,11a,42] As evident from Figure 11, complexes **3** and **4a** reveal a catalytic behavior via two processes: process I at $E_p^{cat} \approx$ -1.78 V for **3** and **4a** and process II at $E_p^{cat} \approx$ -1.91 V or -1.89 V for **3** or **4a**, respectively, where E_p^{cat} is the peak potential of the catalytic waves in Figure 11. The studies of the electrocatalytic properties of **3** and **4a** using the very strong acids HBF_4·Et_2O (pK_a^{DCE} = -10.3, DCE = Dichloroethane)[43] or CF_3SO_3H (pK_a^{DCE} = -11.4)[43] were possible only at low acid concentrations because of the significant direct reduction of these strong acids at the glassy carbon electrode (Figures S-8 to S-10). As shown in Figures S-8 to S-10, protonation follows reduction of **3** or **4a** at low acid concentration and catalysis occurs at potential more negative than that of the primary reduction waves of these model complexes.

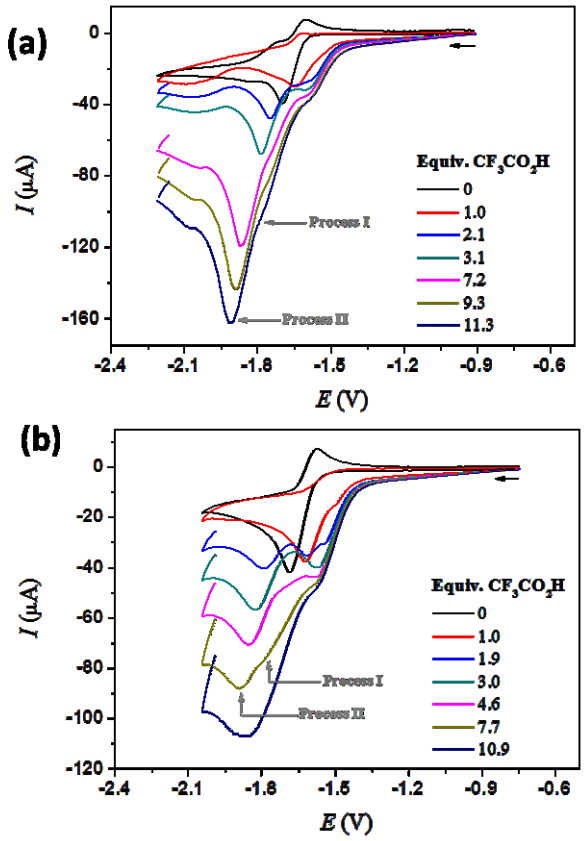

Figure 11. Cyclic voltammetry of complexes (a) 0.632 mM **3** and (b) 0.825 mM **4a** in 0.1 M CH_2Cl_2-[n-Bu_4N][PF_6] solution in the presence of various equivalents of CF_3CO_2H at 0.2 V·s^{-1}. Glassy carbon electrode (A = 0.072 cm^2). E is in V against the Fc^+/Fc couple. The arrows indicate the scan direction.

Conclusions

We report here dinuclear models for the H-cluster featuring unique planarity of their dithiolato linkers (μ-$SCH_2)_2ER_2$ (E = Ge or Sn and R = Me or Ph) and tetranuclear cyclic dimers with a 14-membered ring and unusual temperature dependent ^{1}H NMR spectra. As a result of the repulsive steric interaction between the EMe_2 group and the apical carbonyl ligand in $Fe_2(CO)_6${(μ-$SCH_2)_2EMe_2$} complexes, the central six-membered FeSCECS ring preferentially adopts an unusual conformation with five near-coplanar atoms (– SCECS–) when E = Ge or Sn in dramatic contrast with a chair/boat conformation when E = C or Si. Computations of the complexes in the gas phase support the notion that this near-planarity is the lowest energy conformer. Rings with E = Ge and Sn have less torsional strain and are more deformable than those with E = C. The smaller strain energy also means that the $Fe(CO)_3$ group proximal to the EMe_2 methyl group is less driven to rotate and exchange the apical and basal carbonyl ligands when E = Ge and Sn.

On ionization the reorganization energy of the cation to form the rotated structure with a semibridging CO substantially decreases in the series C through Sn again because of the decreasing release of strain energy down the series. The sulfur ionization energies are substantially lowered as the bridging atom in $Fe_2(CO)_6${(μ-$SCH_2)_2EMe_2$} complexes changes in the series C, Si, Ge, Sn owing to increasing orbital interaction between the σ C–E bond and the S lone pair p-orbital. Consequently, the sulfur character in the HOMO increases down the series. This denotes greater electron-richness of sulfur in the series going from C to Si to Ge to Sn. This increase in the electron density of the [2Fe-2S] core is also reflected by the electrochemical oxidation potentials, where E_{ox} shifts toward less positive values on going from C to Si to Ge to Sn. Nonetheless, the reduction potential $E_{1/2}$ anodically shifts in this series with the Sn-containing complex the easiest to reduce due to diffences in reorganization energy and anion stabilization. Thus, the Sncontaining complex is the easiest to oxidize and reduce.

In the absence of proton source, the complexes $Fe_2(CO)_6${(μ-$SCH_2)_2EMe_2$} (E = Ge or Sn) follow an ECE mechanism of reduction similar to the cases of E = C and Si. These complexes catalyze the reduction of protons from moderate and strong acids.

Experimental Section

Materials and Techniques. All reactions were performed using standard Schlenk and vacuum-line techniques under an inert gas (argon or nitrogen). The ^{1}H and $^{13}C\{^1H\}$ spectra were recorded with a Bruker Avance 200 MHz spectrometer. Chemical shifts are given in parts per million with reference to internal $SiMe_4$ or $CHCl_3$. The mass spectrum was recorded with a Finnigan MAT SSQ 710 instrument. The IR spectra were measured with a Perkin–

Elmer System 2000 FT-IR spectrometer. Elemental analysis was performed with a Leco CHNS-932 apparatus. Silica gel 60 (0.015–0.040 mm) was used for column chromatography, and TLC was performed by using Merck TLC aluminum sheets (Silica gel 60 F254). Solvents from Fisher Scientific and other chemicals from Acros were used without further purification. All solvents were dried and distilled prior to use according to standard methods. The starting materials $(\mu\text{-S})_2Fe_2(CO)_6$[44], $Me_2Ge(CH_2Cl)_2$[45] and $Me_2Sn(CH_2I)_2$[23] were prepared according to literature procedures.

Synthesis of $Ph_2Sn(CH_2I)_2$. Into a 100 mL three-necked round-bottom flask, $Cu(OAc)_2{\cdot}H_2O$ (0.026 g, 0.13 mmol) and CH_3CO_2H (6.0 mL) were mixed and heated to 90-100 °C while stirring. To this hot solution, granular zinc (30-mesh, 1.700 g, 26.0 mmol) was added and the mixture was stirred for 2 min while heating. CH_3CO_2H was removed from the settled Cu-Zn couple using a syringe and fresh CH_3CO_2H (6.0 mL) was added. The mixture was stirred hot for 2 min. CH_3CO_2H was again removed and the couple was cooled, washed with Et_2O (3 × 7.0 mL) and dried by a stream of N_2. The deep grey/black colored couple was covered with THF (7.0 mL) and a few drops of CH_2I_2 were added to initiate the reaction. When the color appears purple, THF (11.0 mL) was added followed by dropwise addition of CH_2I_2 (2.09 mL, 6.96 g, 26.0 mmol) in THF (6.0 mL) using an addition funnel. The addition should be with a rate that maintains the temperature at 40 °C. The addition took 1 h and mild heating was required during the last 15 min. This THF solution of $IZnCH_2I$ was then cooled to ~ 0 °C and filtered under N_2 into a three necked round bottom flask. A solution of diphenyltin dichloride (Ph_2SnCl_2) (1.788 g, 5.2 mmol) in THF (6.0 mL) was added dropwise to the in situ generated $IZnCH_2I$ during 1 h at 40 °C. For an additional 2 h, the reaction mixture was stirred at 40 °C. The cloudy, deep purple reaction mixture was diluted with equal volume of benzene (30 mL), extracted with 5 % HCl (4 × 60.0 mL). The organic phase was dried with Na_2SO_4, concentrated and purified by column chromatography (SiO_2 / hexane:CH_2Cl_2, 1:1) to afford $Ph_2Sn(CH_2I)_2$ (1.393 g, 48 % yield) as a colorless oil containing semi-crystalline particles of the same compound.

DEI-MS (*m*/*z*): 479 $[PhSn(CH_2I)_2]^+$, 415 $[Ph_2SnCH_2I]^+$, 351 $[PhSn(CH_2I)(CH_2)]^+$ and 273 $[Ph_2Sn]^+$. $^{13}C\{^1H\}$ NMR (400.08 MHz, $CDCl_3$): δ –10.53 (s, *C*H_2), 126.0-128.78 (m, CC*H*C*H*CH), 136.85 (m, C*C*HCHCH), 139.31 (m, *C*CHCHCH). ^1H NMR (400.08 MHz, $CDCl_3$): δ 2.41 (s with Sn satellites, $^2J\{^{117}Sn,^1H\}$ = 20.9 Hz, $^2J\{^{119}Sn,^1H\}$ = 41.8 Hz, 4H, C*H*$_2$), 7.38-7.43 (m, 4H, CCHC*H*C*H*), 7.55-7.60 (m, 2H, CC*H*CHCH).

Synthesis of $Fe_2(CO)_6\{\mu\text{-}(SCH_2)_2GeMe_2\}$ (3). A red solution of $(\mu\text{-S}_2)Fe_2(CO)_6$ (150 mg, 0.436 mmol) in THF (10 mL) was cooled to –78 ºC and treated dropwise with Et_3BHLi (0.9 mL, 0.872 mmol, 1.0 M in THF) to give a dark green solution. After stirring the solution for ~ 20 min at –78 ºC, $Me_2Ge(CH_2Cl)_2$ (88 mg, 0.436 mmol) in THF (3 mL) was added. The mixture was stirred for 18 h while slowly warming up to room temperature, giving rise to a dark red solution. Solvent removal was performed under N_2 using a vacuum transfer line. The residue was extracted several times with pentane and the extracts were collected and dried under N_2 using a vacuum transfer line. The red residue was then purified by column chromatography (SiO_2 / hexane) to give complex **3** (31 mg, 15 % yield).

Anal. Calcd for $C_{10}H_{10}Fe_2O_6S_2Ge$: C, 25.30 %; H, 2.12 %; S, 13.51 %. Found: C, 25.28 %; H, 2.14 %; S 13.54 %. Micro-ESI-MS (*m*/*z*): 476 $[M]^+$, 448 $[M - CO]^+$, 420 $[M - 2CO]^+$, 392 $[M - 3CO]^+$, 364 $[M - 4CO]^+$, 334 $[M - 5CO]^+$, 308 $[M - 6CO]^+$. IR (CH_2Cl_2): 1989 (CO), 1996 (CO), 2031 (CO), 2070 (CO) cm^{-1}. $^{13}C\{^1H\}$ NMR (300 MHz, CD_2Cl_2): δ 0.13 (*C*H_3), 6.5 (*C*H_2), 207.95 (*C*O). ^1H NMR (300 MHz, CD_2Cl_2): δ 0.26 (s, 6H, C*H*$_3$), 1.66 (s, 4H, C*H*$_2$).

Synthesis of $Fe_2(CO)_6\{\mu\text{-}(SCH_2)_2SnMe_2\}$ (4a) and $[Fe_2(CO)_6\{\mu\text{-}(SCH_2)_2SnMe_2\}]_2$ (5a). A red solution of $(\mu\text{-S}_2)Fe_2(CO)_6$ (185 mg, 0.538 mmol) in THF (15 mL) was cooled to –78 ºC and treated dropwise with Et_3BHLi (1.0 mL, 1.08 mmol 1.0 M in THF) to give a dark green solution. After stirring the solution for ~ 20 min at –78 ºC, $Me_2Sn(CH_2I)_2$ (184 mg, 0.427 mmol) in THF (3 mL) was added. The mixture was stirred for 18 h while slowly warming up to room temperature, giving rise to a dark red solution. Solvent removal was performed under N_2 using a vacuum transfer line. The residue was extracted several times with pentane and the extracts were collected and dried under N_2 using a vacuum transfer line. The red residue was then purified by column chromatography (SiO_2 / pentane) and two red bands were identified being for **4a** (56 mg, 25 % yield) and **5a** (20 mg, 9 % yield), respectively.

Complex 4a: Anal. Calcd for $C_{10}H_{10}Fe_2O_6S_2Sn$: C, 23.07 %; H, 1.94 %; S, 12.32 %. Found: C, 22.98 %; H, 1.93 %; S 12.36 %. Micro-ESI-MS (*m*/*z*): 520 $[M]^+$. IR (CH_2Cl_2): 2063 (CO), 2031(CO), 1991 (CO), 1974 (CO) cm^{-1}. $^{13}C\{^1H\}$ NMR (200 MHz, CD_2Cl_2): δ –7.1 (*C*H_3), 1.6 (*C*H_2), 207.0 (*C*O). ^1H NMR (200 MHz, CD_2Cl_2): δ 0.25 (s, 6H, C*H*$_3$), 1.79 (s, 4H, C*H*$_2$).

Complex 5a: Anal. Calcd for $C_{20}H_{20}Fe_4O_{12}S_4Sn_2$: C, 23.07 %; H, 1.94 %; S, 12.32 %. Found: C, 23.10 %; H, 1.94 %; S 12.35 %. Micro-ESI-MS (*m*/*z*): 1041 $[M]^+$. FAB-MS (*m*/*z*): 1041, 1013, 957, 929, 901, 873. IR ($CHCl_3$): 2071 (CO), 2031 (CO), 1991 (CO) cm^{-1}. $^{13}C\{^1H\}$NMR (200 MHz, CD_2Cl_2): δ –8.1 (*C*H_3), 1.1 (*C*H_2), 209 (*C*O). ^1H NMR (200 MHz, CD_2Cl_2): δ 0.36 (s, 12H, C*H*$_3$), 2.00 (s, 8H, C*H*$_2$).

Synthesis of $Fe_2(CO)_6\{\mu\text{-}(SCH_2)_2SnPh_2\}$ (4b) and $[Fe_2(CO)_6\{\mu\text{-}(SCH_2)SnPh_2\}]_2$ (5b). A red solution of $(\mu\text{-S}_2)Fe_2(CO)_6$ (95 mg, 0.276 mmol) in THF (15 mL) was cooled to –78 ºC and treated dropwise with Et_3BHLi (0.6 ml, 0.553 mmol, 1.0 M in THF) to give a dark green solution. After stirring the solution for ~ 20 min at –78 ºC, $Ph_2Sn(CH_2I)_2$ (307 mg, 0.553 mmol) in THF (3 mL) was added. The mixture was stirred for 18 h while slowly warming up to room temperature, giving rise to a dark red solution. Solvent removal was performed under N_2 using a vacuum transfer line. The residue was extracted several times with pentane and the extracts were collected and dried under N_2 using a vacuum transfer line. The red residue was then purified by column chromatography (SiO_2 / pentane) and two red bands were identified being for **4b** as a red oil (32 mg, 18 % yield) and **5b** (traces), respectively.

Complex 4b: Anal. Calcd for $C_{20}H_{14}Fe_2O_6S_2Sn$: C, 37.25 %; H, 2.19 %; S, 9.94 %. Found: C, 37.23 %; H, 2.20 %; S 9.96 %. Micro-ESI-MS (*m*/*z*): 646 $[M]^+$. IR (CH_2Cl_2): 2066 (CO), 2032 (CO), 1989 (CO) cm^{-1}. $^{13}C\{^1H\}$ NMR (200 MHz, CD_2Cl_2): δ 1.70 (*C*H_2), 128.7-130.6 (c,d-*C*$_{Ph}$), 136.7-138.7 (a,b-*C*$_{Ph}$), 208.6 (*C*O), 209.1 (*C*O). ^1H NMR (200 MHz, CD_2Cl_2): δ 2.27 (s, 4H, C*H*$_2$), 7.35-7.70 (m, 10H, 2C$_6$*H*$_5$).

Photoelectron Spectroscopy: Photoelectron spectra were recorded using an instrument that features a 360 mm radius hemispherical analyzer (McPherson),[46] with a custom-designed photon source, sample cells, detection, and control electronics. Calibration and data analysis were described previously.[47] All samples sublimed cleanly, with no visible changes in the spectra during data collection after initial observation of ionizations from the diiron compounds. The sublimation temperatures (at 10^{-6} Torr) were 52–77, 64–84 and 62–87 °C for compounds **1**, **2** and **3**, respectively.

Density Functional Theory (DFT) Computations: DFT computations were carried out with the Amsterdam density functional (ADF2014.06) package.[48,49] The geometries and energies were refined in the gas phase and in solution with the PBE functional[50] with dispersion corrections according to the method of Grimme using the BJ damping function (PBE-D3-BJ).[51] All calculations utilized a triple-ζ Slater type orbital (STO) basis set with one

polarization function (TZP) and relativistic effects by the zero-order regular approximation (ZORA).[52,53] The frozen-core approximation was used for the inner core of all heavy atoms. Diffuse density fitting was employed at the quadruple-ζ level with four polarization functions (QZ4P), and the Becke grid was used with 9402 points.[54] Geometries were further optimized in the solvents tetrahydrofuran, dichloromethane, and acetone according to the COSMO model with default parameters.[55] Figures of the optimized geometries and molecular orbital plots were created with the program VMD.[56]

Structure Determinations. The intensity data for the compounds were collected on a Nonius KappaCCD diffractometer using graphitemonochromated Mo-K$_{\alpha}$ radiation. Data were corrected for Lorentz and polarization effects; absorption was taken into account on a semi-empirical basis using multiple-scans[57-59]. The structures were solved by direct methods (SHELXS[60]) and refined by full-matrix least squares techniques against Fo^2 (SHELXL-97[60]). The hydrogen atoms of **3** and **5b** were located by difference Fourier synthesis and refined isotropically. All other hydrogen atoms were included at calculated positions with fixed thermal parameters. All non-hydrogen atoms were refined anisotropically[60]. Crystallographic data as well as structure solution and refinement details are summarized in Table S-4. MERCURY was used for structure representations.

Cyclic Voltammetry. These experiments do not involve corrections for the iR drop. Cyclic voltammetric experiments were performed in a three- electrode cell using a Radiometer potentiostat (μ-Autolab Type-III or an Autolab PGSTAT 12) driven by the GPES software. The working electrode consisted of a vitreous carbon disk (A = 0.072 cm^2) that was polished on a felt tissue with alumina before each CV scan. The Ag/Ag$^+$ reference electrode was separated from the analyte by a CH_2Cl_2–[n-Bu_4N][PF_6] bridge. All the potentials are quoted against the ferrocene-ferrocenium couple (Fc^+/Fc); ferrocene was added as an internal standard at the end of the experiments.

Acknowledgements

The authors (TS, DLL and RSG) gratefully acknowledge support of this work by the U. S. National Science Foundation (Grant No. 1111718 and 1111570). L. A. and H. A. are grateful to the Deutscher Akademischer Austausch Dienst (DAAD) for scholarships. G. M. and W. W. thank the National Science Center (Cracow, PL) for financial support (Grant Maestro-3; Dec-2012/06/A/ST5/00219).

Keywords: hydrogenase • conformational analysis • sulfur • electron-richness • reorganization energies • photoelectron • DFT • Electrocatalysis

[1] a) B. J. Lemon and J. W. Peters, *Biochemistry* **1999**, *38*, 12969–12973; b) A. S. Pandey, T. V. Harris, L. J. Giles, J. W. Peters, R. K. Szilagyi, *J. Am. Chem. Soc.* **2008**, *130*, 4533-4540; c) Y. Nicolet, A. L. de Lacey, X. Vernède, V. M. Fernandez, E. C. Hatchikian, J. C. Fontecilla-Camps, *J. Am. Chem. Soc.* **2001**, *123*, 1596–1601; (d) A. A-Venkatesh, S. Roy, J. F. Siebel, T. R. Simmons, M. Fontecave, V. Artero, E. Reijerse, W. Lubitz, *J. Am. Chem. Soc.* **2015**, *137* (40), 12744-12747.

[2] a) J. W. Peters, W. N. Lanzilotta, B. J. Lemon, L. C. Seefeldt, *Science* **1998**, *282*, 1853-1858; b) Y. Nicolet, C. Piras, P. Legrand, E. C. Hatchikian, J. C. Fontecilla-Camps, *Structure* (London) **1999**, *7*, 13-23; c) H-J. Fan, M. B. Hall, *J. Am. Chem. Soc.* **2001**, *123*, 3828-3829; d) Z-P. Liu, P. Hu, *J. Am. Chem. Soc.* **2002**, *124*, 5175-5182; e) C. Greco, M. Bruschi, L. D. Gioia, U. Ryde, *Inorg. Chem.* **2007**, *46*, 5911-1521; f) S. Trohalaki, R. Pachter, *Int. J. Hydrogen Energy* **2010**, *35*, 5318-5331.

[3] a) W. Dong, M. Wang, X. Liu, K. Jin, G. Li, F. Wang, *Chem. Commun.* **2006**, 305-307; b) S. Ezzaher, A. Gogoll, C. Bruhn, S. Ott, *Chem. Commun.* **2010**, *46*, 5775-5777; c) R. J. Wright, W. Zhang, X. Yang, M. Fasulo, T. D. Tilley, *Dalton Trans.* **2012**, *41*, 73-82; d) R. Zaffaroni, T. B. Rauchfuss, D. L. Gray, L. De Goia, G. Zampelli, *J. Am. Chem. Soc.* **2012**, *134*, 19260-19269; e) R. Goy, L. Bertini, H. Görls, L. De Gioia, J. Talarmin, G. Zampella, P. Schollhammer, W. Weigand, *Chem. Eur. J.* **2015**, *21*, 5061-5073.

[4] M. W. W. Adams, *J. Biol. Chem*. **1987**, *262*, 15054-15061.

[5] a) M. Frey, ChemBioChem **2002**, *3*, 153-160; b) M. Demuez, L. Cournac, O. Guerrini, P. Soucaille, L. Girbal, *FEMS Microbiol. Lett.* **2007**, *275*, 113-121.

[6] a) G. A. N. Felton, C. A. Mebi, B. J. Petro, A. K. Vannucci, D. H. Evans, R. S. Glass, D. L. Lichtenberger, *J. Organomet. Chem.* **2009**, *694*, 2681-2699; b) C. Tard, C. J. Pickett, *Chem. Rev.* **2009**, *109*, 2245-2274; c) J.-F. Capon, F., Gloaguen, F. Y. Petillon, P. Schollhammer, J. Talarmin, *Coord. Chem. Rev*. **2009**, *253*, 1476-1494; d) F. Gloaguen, T. B. Rauchfuss, *Chem. Soc. Rev.* **2009**, *38*, 100-108; e) S. Tschierli, S. Ott, R. Lomoth, *Energy Environ. Sci.* **2011**, *4*, 2340-2352; f) N. Wang, M. Wang, L. Chen, L. Sun, *Dalton Trans.* **2013**, *42*, 12059-12071; g) W. Lubitz, H. Ogata, O. Rüdiger, E. Reijerse *Chem Rev.* **2014**, *114*, 4081-4148; h) T. R. Simmons, G. Berggren, M. Bacchi, M. Fontecave, V. Artero, *Coord. Chem. Rev.* **2014**, *270-271*, 127-150; i) R. Trautwein, L. R. Almazahreh, H. Görls, W. Weigand, *Dalton Trans.* **2015**, *44*, 18780-18794; j) Y. Li, T. B. Rauchfuss, *Chem. Rev*., **2016**, 116, 7043-7077.

[7] a) T. Liu, M. Y. Darensbourg, *J. Am. Chem. Soc*. **2007**, *129*, 7008-7009; b) A. K. Justice, T. B. Rauchfuss, S. R. Wilson, *Angew. Chem. Int. Ed*. **2007**, *46*, 6152-6154; c) A. K. Justice, L. De Gioia, M. J. Wilges, T. B. Rauchfuss, S. R. Wilson, G. Zampella, *Inorg. Chem*. **2008**, *47*, 7405-7414; d) C.-H. Hsieh, O. F. Erdem, S. D. Harman, M. L. Singleton, E. Reijerse, W.Lubitz, C. V. Popescu, J. H. Reibenspies, S. M. Brothers, M. B. Hall, M. Y. Darensbourg, *J. Am. Chem. Soc*. **2012**, *134*, 13089-13102.

[8] a) W. Wang, T. B. Rauchfuss, C. E. Moore, A. L. Rheingold, L. De Gioia, G. Zampella, *Chem. Eur. J.* **2013**, *19*, 15476-15479; b) S. Munary, J.-F.Capon, L. De Gioia, C. Elleouet, C. Greco, F.Y. Petillon, P. Schollhammer, J. Talarmin, G. Zampella, *Chem. Eur. J*. **2013**, *19*, 15458-15461; c) R. Goy, L. Bertini, C. Elleouet, H. Görls, G. Zampella, J. Talarmin, L.Gioia, P. Schollhammer, U.-P. Apfel, W. Weigand, *Dalton Trans*. **2015**, *44*, 1690-1699.

[9] J. W. Tye, M. Y. Darensbourg, M. B. Hall, *Inorg. Chem.* **2006**, *45*, 1552-1559.

[10] a) M. L. Singleton, N. Bhuvanesh, J. H. Reibenspies, M. Y. Darensbourg, *Angew. Chem. Int. Ed.* **2008**, *47*, 9492-9495; b) D. J. Crouthers, J. A. Denny, R. D. Bethel, D. G. Munoz, M. Y. Darensbourg, *Organometallics* **2014**, *33*, 4747-4755.

[11] a) G. A. N. Felton, A. K. Vannucci, J. Chen, L. T. Lockett, N. Okumura, B. J. Petro, U. I. Zakai, D.H. Evans, R. S. Glass, D. L. Lichtenberger, *J. Am. Chem. Soc*. **2007**, *129*, 12521-12530; b) G. A. N. Felton, B. J. Petro, R. S. Glass, D. L. Lichtenberger, D. H. Evans, *J. Am. Chem. Soc.* **2009**, *131*, 11290-11291.

[12] (a) J. D. Lawrence, H. X. Li, T. B. Rauchfuss, M. Benard, M. M. Rohmer, *Angew. Chem., Int. Ed.* **2001**, *40*, 1768-1771; (b) J. -F. Capon, S. Ezzaher, F. Gloaguen, F. Y. Pétillon, P. Schollhammer, J. Talarmin, T. J. Davin, J. E. McGrady, K. W. Muir, *New J. Chem*. **2007**, *31*, 2052-2064; (c) F. Wang, M. Wang, X. Liu, K. Jin, W. Dong, L. Sun, *Dalton Trans*. **2007**, 3812-3819; (d) H. -G. Cui, M. Wang, W. -B. Dong, L. -L. Duan, P. Li, L. –C. Sun, *Polyhedron* **2007**, *26*, 904-910; (e) S. Jiang, J. Liu, L. Sun, *Inorg. Chem. Commun*. **2006**, *9*, 290-292; (f) Z. Wang, J. -H. Liu, , C. -J. He, S. Jiang, B. Åkermark, L. –C. Sun, *J. Organomet. Chem.* **2007**, *692*, 5501-5507; (g) W. -G. Wang, H. -Y. Wang, G. Si, C. -H. Tung, L. –Z. Wu, *Dalton Trans*. **2009**, 2712-2720; (h) Y. Na, M. Wang, J. Pan, P. Zhang, B. Åkermark, L. Sun, *Inorg. Chem*. **2008**, *47*, 2805-2810; (i) Z. Wang, J. Liu, C. He, S. Jiang, B. Åkermark, L. Sun, *Inorg. Chim. Acta* **2007**, *360*, 2411-2419; (j) Y. Si, C. Ma, M. Hu, H. Chen, C. Chen, Q. Liu, *New J. Chem*. **2007**, *31*, 1448-1454; (k) L. Schwartz, G. Eilers, L. Eriksson, A. Gogoll, R.

Lomoth, S. Ott, *Chem. Commun.* **2006**, 520-526; (l) G. Eilers, L. Schwartz, M. Stein, G. Zampella, L. de Gioia, S. Ott, R. Lomoth, *Chem. Eur. J.* **2007**, *13*, 7075-7084; (m) J. Hou, X. Peng, J. Liu, Y. Gao, X. Zhao, S. Gao, K. Han, *Eur. J. Inorg. Chem.* **2006**, 4679-4686; (n) S. Ezzaher, P. -Y. Orain, J. -F. Capon, F. Gloaguen, F. Y. Pétillon, T. Roisnel, P. Schollhammer, J. Talarmin, *Chem. Commun*. **2008**, 2547-2549; (o) M. E. Carroll, B. E. Barton, T. B. Rauchfuss, P. J. Carroll, *J. Am. Chem. Soc.* **2012**, *134*, 18843-18852.

[13] (a) A. Winter, L. Zsolnai, G. Huttner, *Chem. Ber.* **1982**, *115*, 1286-1304; (b) A. Winter, L. Zsolnai, G. Huttner, *Naturforsch.* B **1982**, *37*, 1430-1436; (c) M. L. Singleton, R. M. Jenkins, C. L. Klemashevich, M. Y. Darensbourg, *C. R. Chemie* **2008**, *11*, 861-874; (d) B. E. Barton, M. T. Olsen, T. B. Rauchfuss, *J. Am. Chem. Soc.* **2008**, *130*, 16834-16835; (e) B. E. Barton, T. B. Rauchfuss, *Inorg. Chem.* **2008**, *47*, 2261-2263; (f) R. Trautwein, L. R. Almazahreh, H. Görls, W. Weigand, *Z. Anorg. Allg. Chem.* **2013**, *639*, 1512-1519.

[14] (a) H. X. Li, T. B. Rauchfuss, *J. Am. Chem. Soc*. **2002**, *124*, 726-727; (b) L. -C. Song, Z. -Y. Yang, H. -Z. Bian, Y. Liu, H. -T. Wang, X. -F. Liu, Q. -M. Hu, *Organometallics* **2005**, *24*, 6126-6135.

[15] (a) L. -C. Song, Z. -Y. Yang, Y. -J. Hua, H. -T. Wang, Y. Liu, Q. -M. Hu, *Organometallics* **2007**, *26*, 2106-2110; (b) J. Windhager, M. Rudolph, S. Brautigam, H. Görls, W. Weigand, *Eur. J. Inorg. Chem*. **2007**, 2748-2760; (c) L. –C. Song, A. –G. Zhu, Y. –Q. Guo, *Dalton Trans*. **2016**, *45*, 5021–5029.

[16] M. Harb, Ph.D. Dissertation, Friedrich-Schiller Universität Jena, Jena, Thüringen, **2009**.

[17] U.-P. Apfel, D. Troegel, Y. Halpin, S. Tschierlei, U. Uhlemann, H. Görls, M. Schmitt, J. Popp, P. Dunne, M. Venkatesan, M. Coey, M. Rudolph, G. J. Vos, R. Tacke, W. Weigand, *Inorg. Chem*. **2010**, *49*, 10117-10132.

[18] a) L. R. Almazahreh, U.-P. Apfel, W. Imhof, M. Rudolph, H. Görls, J. Talarmin, P. Schollhammer, M. El-khateeb, W. Weigand, *Organometallics* **2013**, *32*, 4523-4530; b) L. R. Almazahreh, W. Imhof, J. Talarmin, P. Schollhammer, H. Görls, M. Y. El-khateeb, W. Weigand, *Dalton Trans*. **2015**, *44*, 7177-7189.

[19] (a) M. K. Harb, J. Windhager, T. Niksch, H. Görls, T. Sakamoto, E. R. Smith, R. S. Glass, D. L. Lichtenberger, D. H. Evans, M. El-khateeb, W. Weigand, *Tetrahedron* **2012**, *68*, 10592-10599; (b) S. Gao, J. Fan, S. Sun, X. Peng, X. Zhao, J. Hou, *Dalton Trans.* **2008**, 2128-2135; (c) M. K. Harb, U. -P. Apfel, J. Kübel, H. Görls, G. A. N. Felton, T. Sakamoto, D. H. Evans, R. S. Glass, D. L. Lichtenberger, M. El-khateeb, W. Weigand, *Organometallics* **2009**, *28*, 66666675; (d) U. -P. Apfel, H. Görls, G. A. N. Felton, D. H. Evans, R. S. Glass, D. L. Lichtenberger, W. Weigand, *Helv. Chim. Acta* **2012**, *95*, 2168-2175.

[20] (a) P. Das, J. -F. Capon, F. Gloaguen, F. Y. Pétillon, P. Schollhammer, J. Talarmin, K. W. Muir, *Inorg. Chem.* **2004**, *43*, 8203-8205; (b) L. –C. Song, Z. –C. Gu, W. –W., Q. –L. Li, Y. –X. Wang, H. -F. Wang, *Organometallics* **2015**, *34*, 4147-4157.

[21] R. S. Glass, N. E. Gruhn, E. Lorance, M. S. Singh, N. Y T. Stessman, U. I. Zakai, *Inorg. Chem.* **2005**, *44*, 5728-5737.

[22] a) R. S. Glass, A. M. Radspinner, W. P. Singh, *J. Am. Chem. Soc.* **1992**, *114*, 4921-4923; b) R. S. Glass, Q. Guo, Y. Liu, *Tetrahedron* **1997**, *53*, 1227312286; c) R. S. Glass, E. Block, N. E. Gruhn, J. Jin, E. Lorance, U. I. Zakai, S.-Z. Zhang, *J. Org. Chem.* **2007**, *72*, 8290-8297.

[23] D. Seyferth, S. B. Andrews, *J. Organomet. Chem.* **1971**, *30*, 151-166.

[24] Y. Nicolet, A. L. de Lacey, X. Vernede, V. M. Fernandez, C. E. Hatchikian, J. C. Fontecilla-Camps, *J. Am. Chem. Soc.* **2001**, *123*, 1596-1602.

[25] N. L. Allinger, X. Zhou, John Bergsma, *J. Mol. Struct. Theochem* **1994**, *312*, 69-83.

[26] A. K. Rappé, C. J. Casewit, K. S. Colwell, W. A. Goddard III, W. M. Skiff, *J. Am. Chem. Soc.* **1992**, *114*, 10024-10035.

[27] E.J. Lyon, I.P. Georgakaki, J.H. Reibenspies, M.Y. Darensbourg, *J. Am. Chem. Soc.* **2001**, *123*, 3268-3278.

[28] a) J. B. Hendrickson, *J. Am, Chem. Soc.* **1961**, *83*, 4537-4547; b) D. J. Nelson, C. N. Brammer, *J. Chem. Ed.* **2011**, *88*, 292-294.

[29] a) C. H. Bushweller, in "Conformational Behavior of Six-Membered Rings," Juaristi, E., Ed., VCHNY, 1995; b) D. A. Dixon, A. Komornicki, *J. Phys. Chem.* **1990**, *94*, 5630-5636; c) C. A. Stortz, *J. Phys. Org. Chem*. **2010**, *23*, 1173-1186.

[30] K. Kakhiani, U. Lourdera, W. Hu, D. Birney, W. L. Hase, *J. Phys. Chem. A* **2009**, *113*, 4570-4580.

[31] F. A. L. Anet, A. J. R. Bourn, *J. Am. Chem. Soc.* **1967**, *89*, 760-768.

[32] R. J. Ouellette, *J. Am. Chem. Soc*. **1974**, *96*, 2421-2425.

[33] a) M. J. O. Anteunis, R. Dedeyne, *Org. Magn. Reson.* **1977**, *9*, 127-132, b) F. Freeman, C. Cha, C. Fang, A. C. Huang, J. H. Hwang, P.L. Louie, B. A. Shainyan, *J. Phys. Org. Chem.* **2005**, *18*, 35-48; c) S. V. Kirpichenko, E. Kleinpeter, B. A. Shainyan, *J. Phys. Org. Chem.* **2010**, *23*, 859-865.

[34] a) Y. Takeuchi, Y. Ichikawa, K. Tanaka, N. Kakimoto, *Bull. Chem. Soc. Jpn*.**1988**, *61*, 2875-2880; b) Y. Takeuchi, K. Tanaka, T. Harazono, S. Yoshimura, *Bull. Chem. Soc. Jpn.* **1990**, *63*, 708-715; c) Y. Takeuchi, M. Shimoda, K. Tanaka, S. Tomoda, K. Ogawa, H. Suzuki, *J. Chem. Soc., Perkin 2* **1988**, 7-13; d) K.-H. Chen, N. L. Allinger, *J. Phys. Org. Chem*. **1999**, *12*, 528-540.

[35] F. Freeman, C. Fang, D. V. Hoang, K. M. Trinh, *Int. J. Quantum Chem.* **2005**, *105*, 416-428.

[36] a) M. K. Harb, J. Windhager, A. Daraosheh, H. Görls, L. T. Lockett, N. Okumura, D. H. Evans, R. S. Glass, D. L. Lichtenberger, M. El-khateeb, W. Weigand, *Eur. J. Inorg. Chem.* **2009**, 3414-3420; b) M. K. Harb, M. K.; H. Görls, T. Sakamoto, G. A. N. Felton, D. H. Evans, R. S. Glass, D. L. Lichtenberger, M. Elkhateeb, W. Weigand, *Eur. J. Inorg. Chem.* **2010**, 3976-3985; c) M. K. Harb, T. Niksch, J. Windhager, H. Görls, R. Holze, L. T. Lockett, N. Okumura, D. H. Evans, R. S. Glass, D. L. Lichtenberger, M. El-khateeb, W. Weigand, *Organometallics* **2009**, *28*, 1039-1048.

[37] a) L. –C. Song, F. –H. Gong, T. Meng, J. –H. Ge, L. –N. Cui, Q. –M. Hu, *Organometallics* **2004**, *23*, 823-831; b) L. –C. Song, J. –Y. Wang, F. –H. Gong, J. Cheng, Q. –M. Hu, *J. Organomet. Chem*. **2004**, *689*, 930-935; c) M. -H. Chiang, Y. -C. Liu, S. -T. Yang, G.-H. Lee, *Inorg. Chem.* **2009**, *48*, 7604-7612; d) M. K. Harb, A. Daraosheh, H. Görls, E. R. Smith, G. J. Meyer, M. T. Swenson, T. Sakamoto, R. S. Glass, D. L. Lichtenberger, D. H. Evans, M. El-khateeb, W. Weigand, *Heteroat. Chem*. **2014**, *25*, 592-606.

[38] The ^{1}H NMR spectrum of *a,e*-(μ-$CH_3HgS)_2Fe_2(CO)_6$ shows that the nonequivalent methyl groups have the same chemical shifts: Mak, T. C. W.; Book, L.; Chieh, C.; Gallagher, M.K.; Song, L. -C.; Seyferth, D. *Inorg. Chim. Acta,* **1983**, *73*, 159-164. However, the chemical shifts for the nonequivalent methyl protons in **4** differ by 0.10 ppm and the nonequivalent CH_2 protons by 0.46 ppm.

[39] R. S. Nicholson, I. Shain, Anal. Chem. **1965**, *37*, 178-190.

[40] D. Chouffai, J-F. Capon, L. De Gioia, F. Y. Pétillon, P. Schollhammer, J. Talarmin, G. Zampella, *Inorg. Chem*. **2015**, *54*, 299-311.

[41] K. Izutsu, Acid-Base Dissociation Constants in Dipolar Aprotic Solvents, Blackwell Scientific Publications, Oxford, **1990**, vol. 35.

[42] S. J. Borg, S. K. Ibrahim, C. J. Pickett and S. P. Best, *C. R. Chim.* **2008**, *11*, 852-860.

[43] A. Kütt, T. Rodima, J. Saame, E. Raamat, V. Mäemets, I. Kaljurand, I. A. Koppel, R. Yu. Garlyauskayte, Y. L. Yagupolskii, L. M. Yagupolskii, E. Bernhardt, H. Willner, I. Leito, *J. Org. Chem.* **2011**, *76*, 391-395.

[44] P. F. Brandt, D. A. Lesch, P. R. Stafford, T. B. Rauchfuss, *Inorg. Synth.* **1997**, *31*, 112-116.

[45] a) R. Tacke, S. A. Wagner, J. Sperlich, *Chem. Ber.* **1994**, *127*, 639-642; b) J. Barrau, G. Rima, J. Satgé, *Synth. React. Inorg. Met.-Org. Chem.* **1984**, *14* (1), 21-37.

[46] K. Siegbahn, C. Nordling, A. Fahlman, R. Nordberg, *ESCA: Atomic, Molecular and Solid State Structure Studied by Means of Electron Spectroscopy;* Uppsala, Almqvist & Wiksells: **1967**.

[47] M. A. Cranswick, A. Dawson, J. J. A. Cooney, N. E. Gruhn, D. L. Lichtenberger, J. H. Enemark, *Inorg. Chem.* **2007**, *46*, 10639-10646.

[48] G. Te Velde, F. M. Bickelhaupt, E. J. Baerends, C. Fonseca Guerra, S. J. A. Van Gisbergen, J. G. Snijders, T. Ziegler, *J. Comput. Chem.* **2001**, *22*, 931967.

[49] ADF2014.06, scm.com.

[50] J. P. Perdew, K. Burke, M. Ernzerhof, *Phys. Rev. Lett.* **1996**, *77*, 3865-3868.

[51] S. Grimme, S. Ehrlich, L. Goerigk, *J. Comput. Chem.* **2011**, *32*, 1456-1465.

[52] E. van Lenthe, E. J. Baerends, J. G. Snijders, *J. Chem. Phys.* **1993**, *99*, 4597-4610.

[53] E. van Lenthe, A. Ehlers, E. J. Baerends, *J. Chem. Phys.* **1999,** *110*, 8943-8953.
[54] M. Franchini, P.H.T. Philipsen, L. Visscher, *J. Comp. Chem.* **2013**, *34*, 1819-1827.
[55] a) C. C. Pye, T. Ziegler, Theor. Chem. Acc. **1999**, *101*, 396; b) A. Klamt, G. Schüürmann, *J. Chem. Soc., Perkin Trans.* **1993**, *2*, 799-805.
[56] W. Humphrey, A. Dalke, K. Schulten, *J. Molec. Graphics* **1996**, *14*, 33-38. [57] COLLECT, Data Collection Software; Nonius B.V., Netherlands, **1998**.
[58] „Processing of X-Ray Diffraction Data Collected in Oscillation Mode":Otwinowski, Z.; Minor, W. in Carter, C. W.; Sweet, R. M. (eds.): *Methods in Enzymology, Vol. 276, Macromolecular Crystallography, Part A*, pp. 307-326, Academic Press **1997**.
[59] SADABS 2.10, Bruker-AXS inc., **2002**, Madison, WI, U.S.A.
[60] Sheldrick, G. M. *Acta Cryst.* **2008**, *A64*, 112-122.

Entry for the Table of Contents (Please choose one layout)

Layout 1:

FULL PAPER

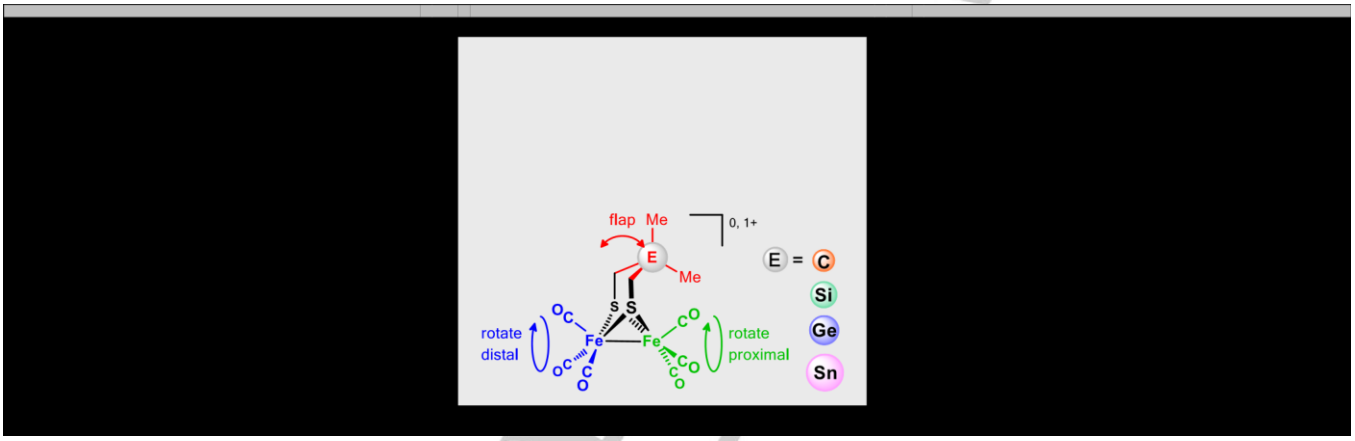

Layout 2:

FULL PAPER

((Insert TOC Graphic here; max. width: 11.5 cm; max. height: 2.5 cm))

*Author(s), Corresponding Author(s)**

Page No. – Page No.

Title